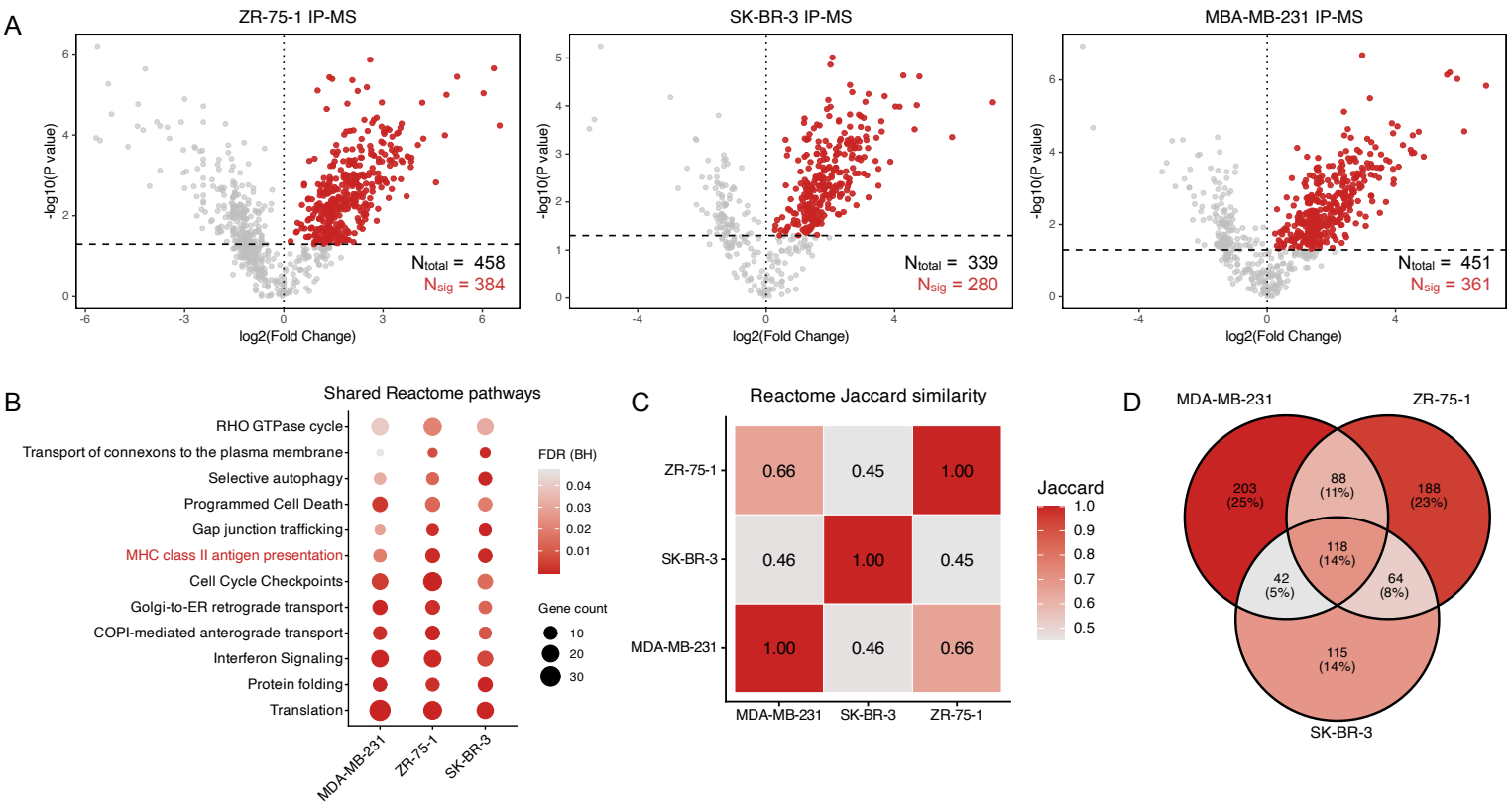


Figure S1. Mapping the tumor-specific MHC-II (tsMHC-II) molecular interactome in breast cancer cells.

A. Volcano plots of tsMHC-II binding proteins identified in three cell lines. $P < 0.05$ was considered significant.

B. Shared Reactome pathway enrichments in all three cell lines.

C. Jaccard similarity score of Reactome pathway enrichments between cell lines.

D. Venn plot of shared tsMHC-II binding proteins identified from all three cell lines.

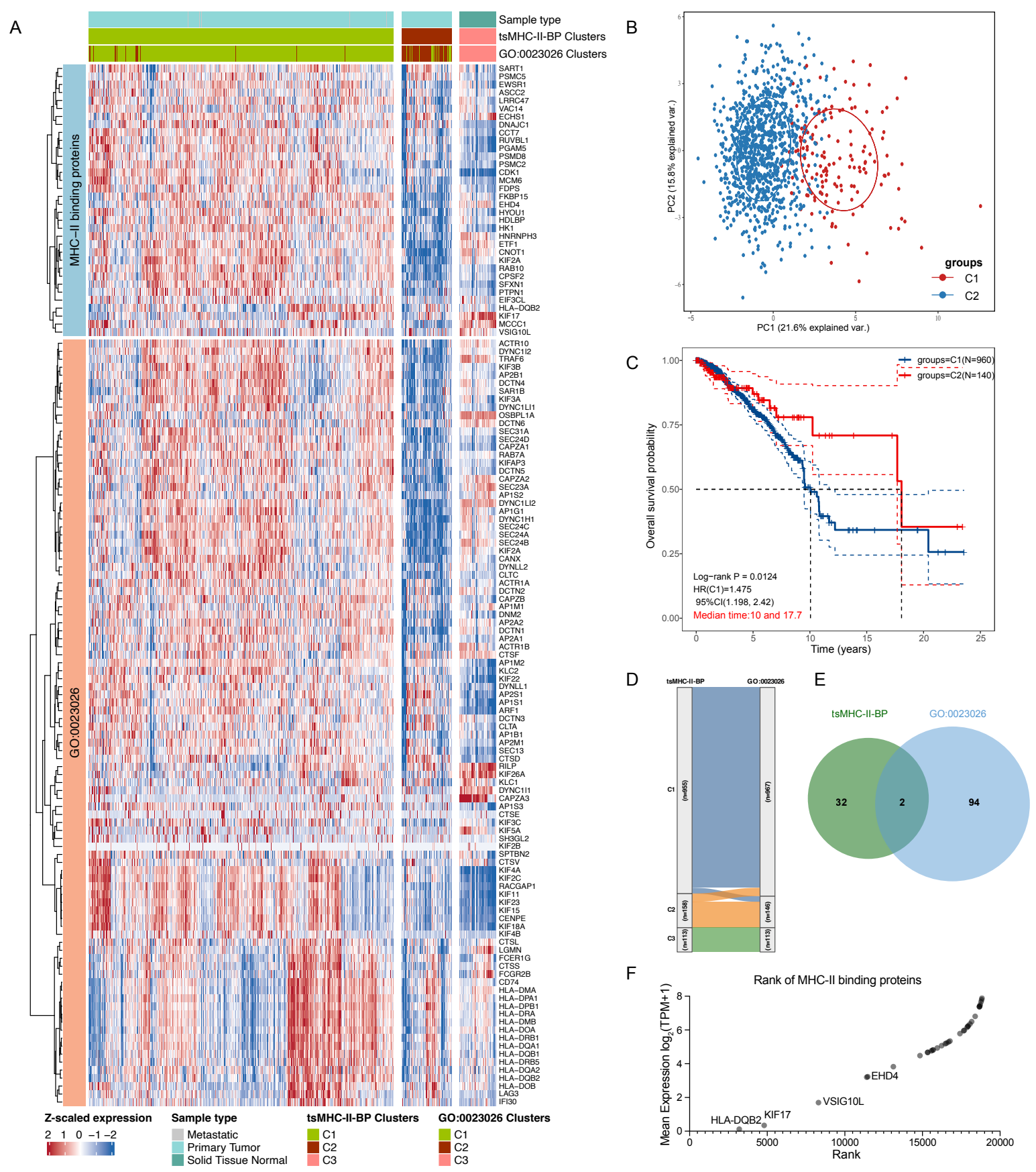


Figure S2. KIF17 ablation is the rate-limiting step in the intracellular trafficking of tsMHC-II.

A. Consensus clustering of TCGA-BRCA tumor patients based on the expressional profile of tsMHC-II-BPs and GO:0023026 genes.

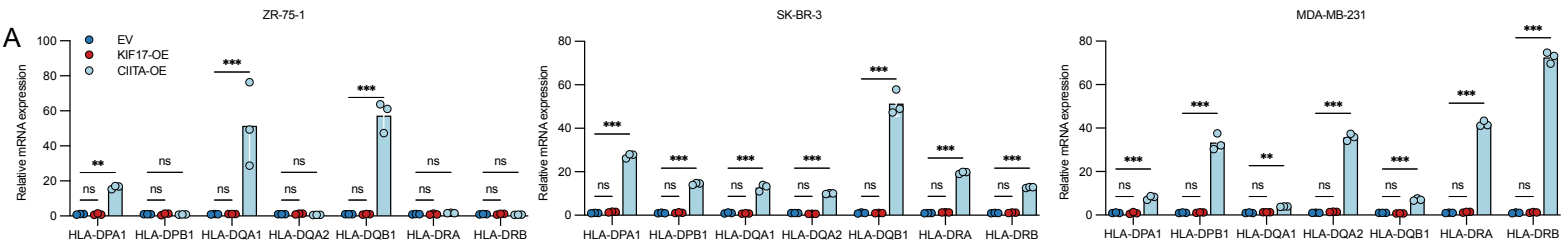
B. Principle component analysis (PCA) of TCGA-BRCA tumor patients based on the expressional profile of GO:0023026 genes.

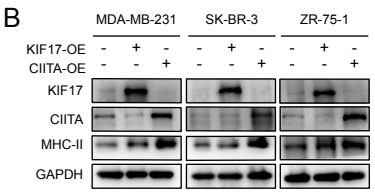
C. Overall survival analysis of t GO:0023026 based clustering of TCGA-BRCA patients, comparison was made by log-rank test.

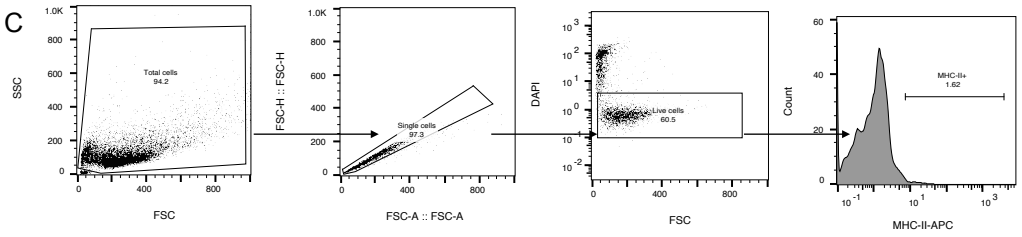
D. Comparison of tsMHC-II-BPs and GO:0023026 based clustering results.

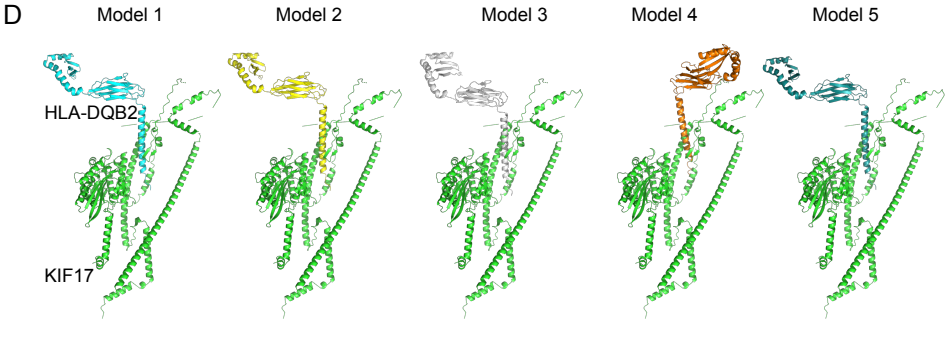
E. Comparison of shared genes between tsMHC-II-BPs and GO:0023026 annotated genes.

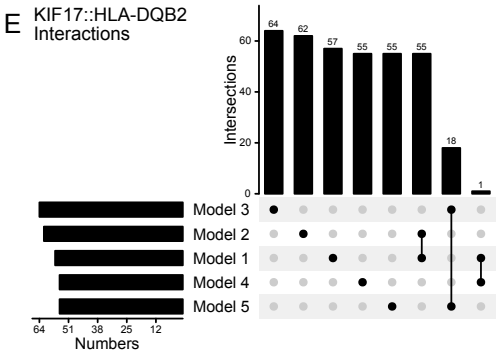
F. Ranking of tsMHC-II-BPs based on the average expression of breast cancer cell lines from CCLE dataset.

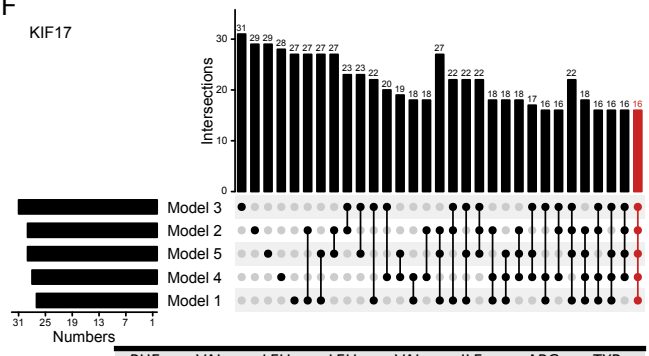




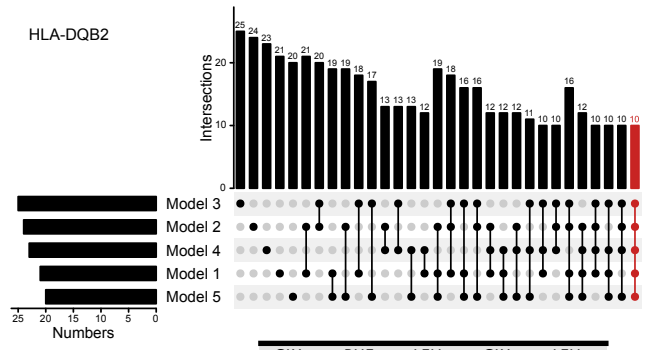




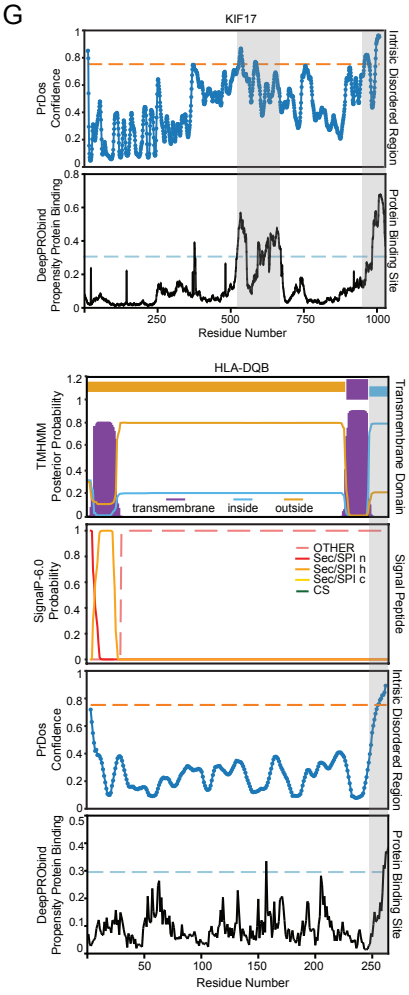




PHE	VAL	LEU	LEU	VAL	ILE	ARG	TYR
616	619	857	861	864	868	869	874
LEU	ILE	LEU	TRP	GLY	TRP	ILE	ILE
877	880	881	886	891	893	895	900



GLY	PHE	LEU	GLY	LEU
240A	243A	244A	245A	246A
LEU	ILE	HIS	ARG	LYS
248A	249A	252A	253A	256A



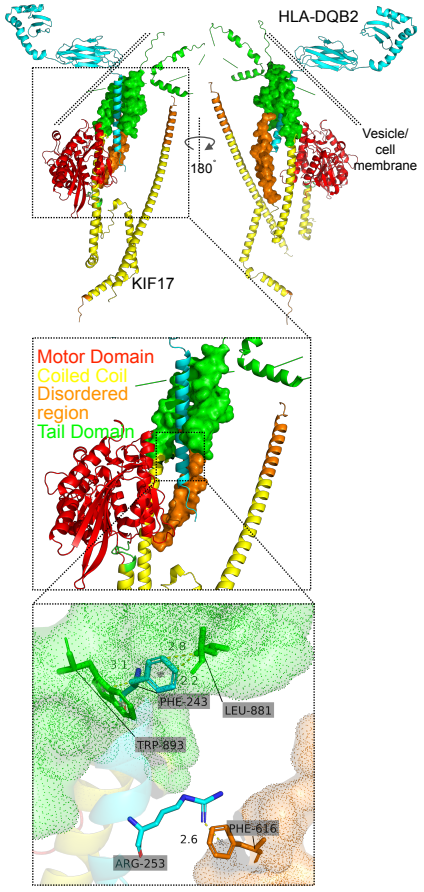


Figure S3. KIF17 facilitates the membrane trafficking of tsMHC-II by directly binding with HLA-DQB2.

A. RNA expression of MHC-II component comparing wild type (WT), KIF17/CIITA over expression (OE) groups using qPCR.

B. .Protein level of tsMHC-II induced by KIF17/CIITA OE.

C. .Gating strategy of the flow cytometry based membrane tsMHC-II measurements.

D. Protein-protein interaction docking of the top 5 models between KIF17 and HLA-DQB2.

E. .Shared KIF17::HLA-DQB2 interactions between the top 5 models.

F. Shared interactive sites of KIF17 and HLA-DQB2 of the top 5 models, respectively.

G. Protein structure prediction of KIF17 and HLA-DQB2.

H. Protein-protein interaction docking of the top 1 models between KIF17 and HLA-DQB2, with each KIF17 domain colored differently.

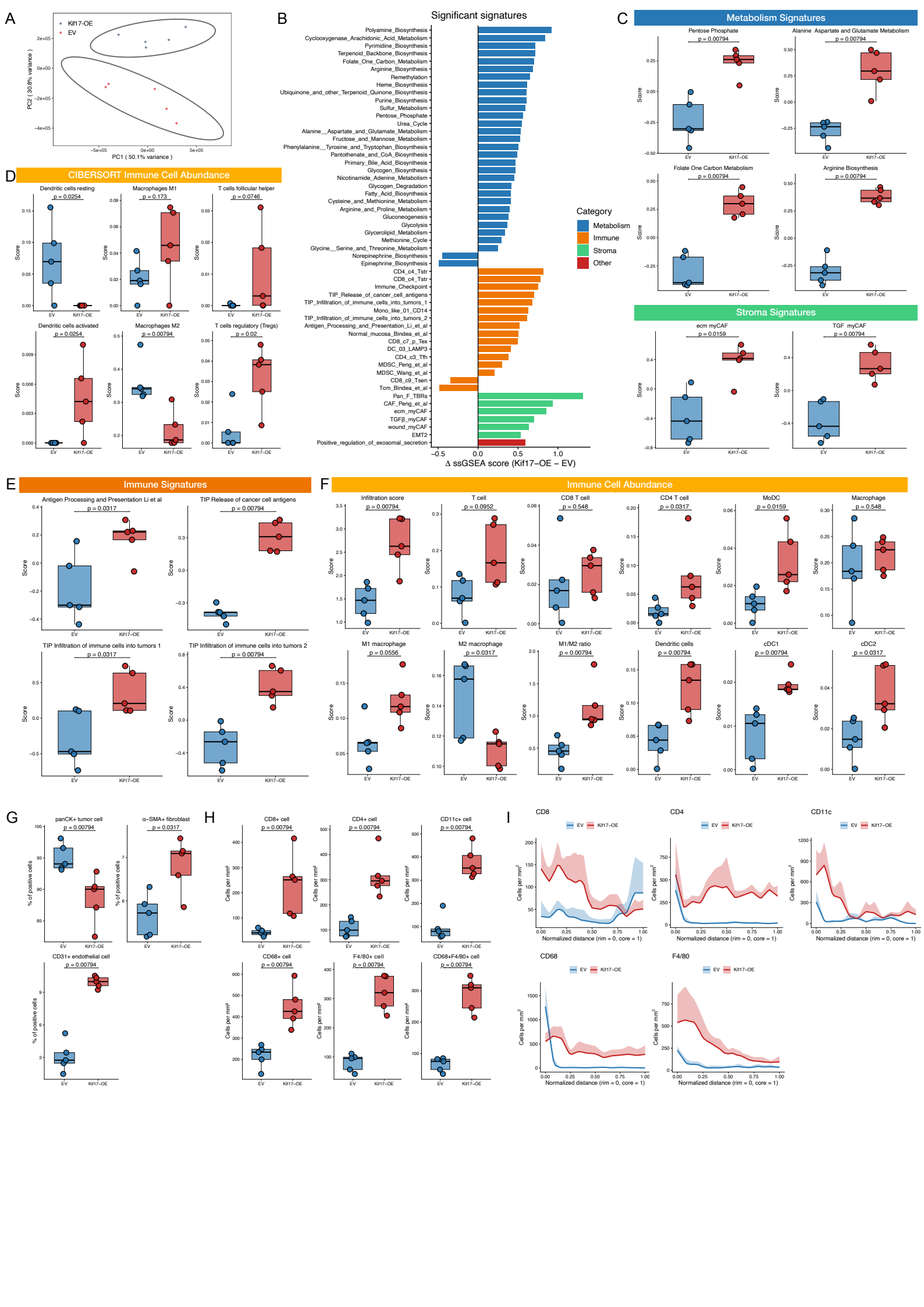

A
Kif17-OE
EV
PC2 (30.8% variance)
PC1 (50.1% variance)
B
Significant signatures
Polyamine_Biosynthesis
Cyclooxygenase_Arachidonic_Acid_Metabolism
Pyrimidine_Biosynthesis
Terpenoid_Backbone_Biosynthesis
Folate_One_Carbon_Metabolism
Arginine_Biosynthesis
Remethylation
Heme_Biosynthesis
Ubiquinone_and_other_Terpenoid_Quinone_Biosynthesis
Purine_Biosynthesis
Sulfur_Metabolism
Pentose_Phosphate
Urea_Cycle
Alanine__Aspartate_and_Glutamate_Metabolism
Fructose_and_Mannose_Metabolism
Phenylalanine__Tyrosine_and_Tryptophan_Biosynthesis
Pantothenate_and_CoA_Biosynthesis
Primary_Bile_Acid_Biosynthesis
Glycogen_Biosynthesis
Nicotinamide_Adenine_Metabolism
Glycogen_Degradation
Fatty_Acid_Biosynthesis
Cysteine_and_Methionine_Metabolism
Arginine_and_Proline_Metabolism
Gluconeogenesis
Glycolysis
Glycerolipid_Metabolism
Methionine_Cycle
Glycine__Serine_and_Threonine_Metabolism
Norepinephrine_Biosynthesis
Epinephrine_Biosynthesis
CD4_c4_Tstr
CD8_c4_Tstr
Immune_Checkpoint
TIP_Release_of_cancer_cell_antigens
TIP_Infiltration_of_immune_cells_into_tumors_1
Mono_like_01_CD14
TIP_Infiltration_of_immune_cells_into_tumors_2
Antigen_Processing_and_Presentation_Li_et_al
Normal_mucosa_Bindea_et_al
CD8_c7_p_Tex
DC_03_LAMP3
CD4_c3_Tfh
MDSC_Peng_et_al
MDSC_Wang_et_al
CD8_c9_Tsen
Tcm_Bindea_et_al
Pan_F_TBRs
CAF_Peng_et_al
ecm_myCAF
TGFβ_myCAF
wound_myCAF
EMT2
Positive_regulation_of_exosomal_secretion
Category
Metabolism
Immune
Stroma
Other
Δ ssGSEA score (Kif17−OE − EV)
C
Metabolism Signatures
Pentose Phosphate
p = 0.00794
Alanine Aspartate and Glutamate Metabolism
p = 0.00794
Folate One Carbon Metabolism
p = 0.00794
Arginine Biosynthesis
p = 0.00794
Stroma Signatures
ecm myCAF
p = 0.0159
TGF myCAF
p = 0.00794
D
CIBERSORT Immune Cell Abundance
Dendritic cells resting
p = 0.0254
Macrophages M1
p = 0.173
T cells follicular helper
p = 0.0746
Dendritic cells activated
p = 0.0254
Macrophages M2
p = 0.00794
T cells regulatory (Tregs)
p = 0.02
E
Immune Signatures
Antigen Processing and Presentation Li et al
p = 0.0317
TIP Release of cancer cell antigens
p = 0.00794
TIP Infiltration of immune cells into tumors 1
p = 0.0317
TIP Infiltration of immune cells into tumors 2
p = 0.00794
F
Immune Cell Abundance
Infiltration score
p = 0.00794
T cell
p = 0.0952
CD8 T cell
p = 0.548
CD4 T cell
p = 0.0317
MoDC
p = 0.0159
Macrophage
p = 0.548
M1 macrophage
p = 0.0556
M2 macrophage
p = 0.0317
M1/M2 ratio
p = 0.00794
Dendritic cells
p = 0.00794
cDC1
p = 0.00794
cDC2
p = 0.0317
G
panCK+ tumor cell
p = 0.00794
α−SMA+ fibroblast
p = 0.0317
CD31+ endothelial cell
p = 0.00794
% of positive cells
H
CD8+ cell
p = 0.00794
CD4+ cell
p = 0.00794
CD11c+ cell
p = 0.00794
CD68+ cell
p = 0.00794
F4/80+ cell
p = 0.00794
CD68+F4/80+ cell
p = 0.00794
Cells per mm²
I
CD8
CD4
CD11c
CD68
F4/80
EV
Kif17−OE
Cells per mm²
Normalized distance (rim = 0, core = 1)

Figure S4. KIF17 overexpression reshapes the tumor immune microenvironment and induces spatial stromal–immune reorganization.

A. PCA of mice RNAseq samples.

B. Global changes in transcriptional signatures between EV and Kif17-OE tumors. All significantly altered signatures identified by ssGSEA analysis are shown and grouped into immune, stroma, metabolism, and other categories. The x-axis represents the difference in ssGSEA scores (ΔssGSEA) between Kif17-OE and EV tumors.

C. Comparison of metabolic and stromal ssGSEA scores between EV and Kif17-OE tumors. Box plots show selected metabolic and stromal signatures inferred from bulk RNA-seq data using ssGSEA. Statistical comparisons between groups were performed using unpaired two-tailed Student's *t*-test.

D. CIBERSORT-based validation of immune cell abundance differences between EV and Kif17-OE tumors.

E. Up-regulation of immune-related transcriptional signatures in Kif17-OE 4T1 tumors. Box plots show representative immune signatures inferred from bulk RNA-seq data using the IOBR package. Statistical comparisons were performed between groups using unpaired two-tailed Student's t-test.

F. Enhanced infiltration of T cells and antigen-presenting cells in Kif17-OE 4T1 tumors. Box plots show inferred immune cell abundance scores, including total immune infiltration, T cells ($CD4^+$, $CD8^+$, Treg, T helper), macrophage subsets (M1, M2, M1/M2 ratio), and dendritic cell populations (total DCs, cDC1, cDC2), estimated from bulk RNA-seq data using the IOBR package. Statistical comparisons were performed between groups using unpaired two-tailed Student's t-test.

G. Quantification of tumor cell (panCK+), fibroblast (αSMA+) and endothelial cells (CD31+) shown in Figure 4E.

H. Quantification of immune cell populations shown in Figure 4F expressed as cell density (cells per mm^2).

I. Quantification of immune cell populations shown in Figure 4G using cell density (cells per mm^2) across 200 μm concentric bands from the tumor rim to the core. Spatial distance was normalized from rim (0) to core (1). Results are consistent with the percentage-based spatial analysis shown in Figure 4G.

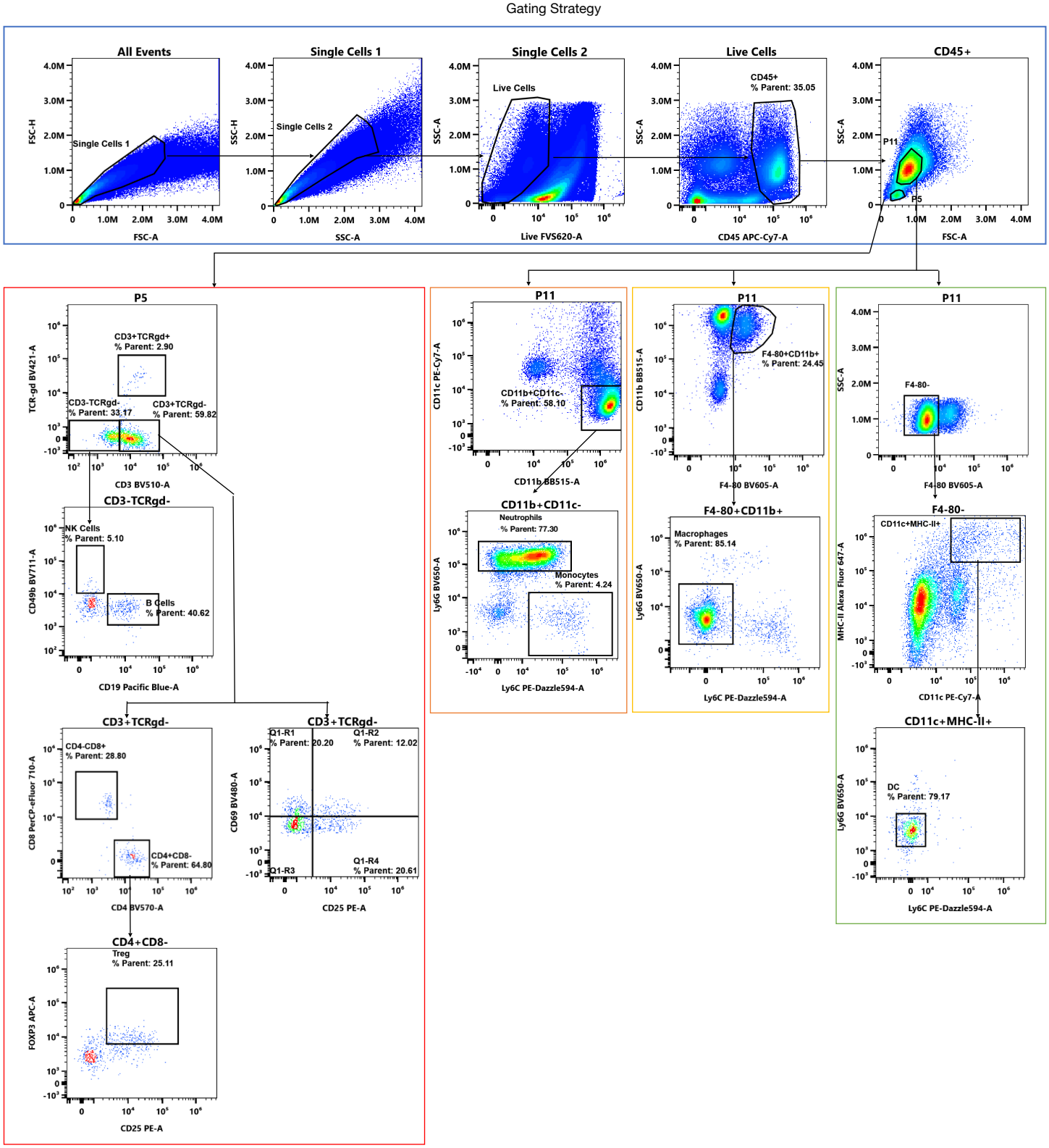


Figure S5. Multiplex spectral flow cytometry gating strategy. Following tumor dissociation, singlets and live cells were sequentially gated before selection of CD45+ immune cells. Lymphoid populations including γδ T cells, conventional αβ T cells, CD4+ T cells, CD8+ T cells, Tregs, NK cells, and B cells were identified based on lineage-marker expression and activation states. Myeloid populations including neutrophils, monocytes, macrophages, and dendritic cells (DCs) were further defined using CD11b, F4/80, CD11c, Ly6G, Ly6C, and MHC-II expression. Representative gating plots are shown.